A method for registration and model-based segmentation of Doppler ultrasound images

Hrvoje Kalinić[a], Sven Lončarić[a], Maja Čikeš[b], Davor Miličić[b], Ivo Čikeš[b], George Sutherland[c], Bart Bijnens[d]
[a]Faculty of Electrical Engineering and Computing, Unska 3, Zagreb, Croatia
[b]University Hospital Centre Rebro, Zagreb, Croatia [c]St. George's Hospital, London, United Kingdom [d]Universitat Pompeu Fabra, Barcelona, Spain

ABSTRACT

Morphological changes of Doppler ultrasound images are an important source of information for diagnosis of cardiovascular diseases. Quantification of these flow profiles requires segmentation of the ultrasound images. In this article, we propose a new model-based method for segmentation of (aortic outflow) velocity profiles. The method is based on a procedure for registration using a geometric transformation specifically designed for matching Doppler ultrasound profiles. After manual segmentation of a model image, the model image is temporally registered to a new image using two manually defined points in time. Next, a non-rigid registration was carried out in the velocity direction. As a similarity measure normalized mutual information is used, while optimization is performed by a genetic algorithm. The registration method is experimentally validated using an in-silico image phantom, and showed an accuracy of 5.4%. The model based segmentation is evaluated in a series of aortic outflow Doppler ultrasound images from 30 normal volunteers. Comparing the automated method to the manual delineation by an expert cardiologist the method proved accurate to 6.6%. The experimental results confirm the accuracy of the approach and shows that the method can be used for the segmentation of clinically obtained aortic outflow velocity profiles.

1. INTRODUCTION

Doppler ultrasound blood flow profiles are clinically important for the diagnosis of cardiovascular diseases. Blood velocities over the mitral valve provide information on filling of the ventricles (diastolic function), while aortic outflow velocities contain information on cardiac function.[1] Thus, the quantification of the morphological changes in the velocity profiles over the valves are linked to cardiovascular diseases and are of clinical importance.[2,3] To facilitate the quantitative analysis, it is required to extract the velocity profile from the Doppler ultrasound image using a segmentation method. When studying aortic outflow velocities, it is possible to extract clinically relevant features that characterize the profile shape.[4] However, manual segmentation is a time consuming task, therefore an automatic segmentation procedure is preferable.

In this paper, we present a method for model-based segmentation of aortic outflow velocity profiles, which utilizes a new method for registration of Doppler ultrasound images. The registration procedure described in the next section is used for the model-based segmentation. Since one of the images from the set was used as a model we will further refer to this image as the reference image. The reference image is manually segmented by

Further author information: (Send correspondence to H.K.)
H.K.: Adress: Faculty of Electrical Engineering and Computing, Department of Electronic Systems and Information Processing, Universiy of Zagreb, 10000 Zagreb, Croatia; Email to: hrvoje.kalinic@fer.hr; Telephone +38616129940; ipg.zesoi.fer.hr
S.L.: Adress: Faculty of Electrical Engineering and Computing, Department of Electronic Systems and Information Processing, Universiy of Zagreb, 10000 Zagreb, Croatia
M.Č.: Adress: Department for Cardiovascular Diseases, University Hospital Centre Zagreb, 10000 Zagreb, Croatia
D.M.: Adress: Department for Cardiovascular Diseases, University Hospital Centre Zagreb, 10000 Zagreb, Croatia
G.S.: Adress: St. George's Hospital, Cardiology, SW17 0QT London, UK
B.B.: Adress: Catalan Institution for Research and Advanced Studies (ICREA) and Universitat Pompeu Fabra (CISTIB), E08003 Barcelona, Spain

an expert cardiologist to obtain the reference outflow profile. Later, this reference profile is transformed to the target patient image to obtain the segmentation.

The registration and resulting segmentation method are specifically targeted for processing ultrasound Doppler velocity profiles. The accuracy of the registration is tested in an (in-silico) phantom while the whole segmentation method is evaluated in a set of clinical aortic outflow images.

2. METHODS

2.1 Registration

The goal of image registration is to determine parameters of the geometric transformation, which maps a source image into a target image. The source and the target images will be denoted as $S(\overrightarrow{x})$ and $T(\overrightarrow{x})$, respectively, where $\overrightarrow{x}$ will be used as vector defined by the ordered pair in a Cartesian coordinate system, i.e. (x, y).

Doppler ultrasound images represent the instantaneous blood velocity within the sample volume (pulsed Doppler) or scan line (continuous wave Doppler) as a function of time, referenced to the heart cycle using the electrocardiogram. This implies that the relevant phase of the cardiac cycle has to be extracted (the ejection period when quantifying aortic outflow) and that the changes in the instantaneous velocities have to be quantified. This acctually describes the transformation needed to register Doppler images, which consists out of two parts. The first part is denoted as $e(\overrightarrow{x})$ and represents the extracting the relevant phase of the cardiac cycle and scaling of the source image to the target image to obtain the same resolution. This part of image registration is done semi-automatically since it uses manually identified phase cycle. The second part of the image registration process is denoted as $f(\overrightarrow{x})$ and it is non-rigid transformation. The total transformation of an image can therefore be written as:

$$(f \circ e)(\overrightarrow{x}). \tag{1}$$

Since the mayor information in the outflow velocity profile is in the changes in the instantaneous velocities, the mayor difference between outflow velocity profiles are in the y-axis (velocity) direction. Thus, after identifying the phase in the cycle, the possible inter-individual changes in the profile can be described with a one-dimensional transformation on the velocity scale. The transformation $f(\overrightarrow{x})$ can therefore be reduced to the transformation $f(x)$ since it is only the function of the variable x (corresponding to time). For the sake of notation simplicity we will observe the case when all the images are already scaled to same resolution (i.e. transformation e is done), and further talk of $f(x)$ as an transformation function.

To calculate this transformation function, the image $S(\overrightarrow{x})$ is divided in N vertical segments and each of these is scaled with a different scaling factor. These scaling factors together define the transformation vector noted by t. Continuity of the transformation function $f(x)$ is obtained using a cubic spline interpolation, thus avoiding the discontinuities between adjacent segments. If one selects $N = 10$, this can be depicted as shown in Figure 1. The left image shows an image divided in ten segments where each segment is scaled with respect to its scaling factor. The right image shows the same image where the scaling of each stripe is done using transformation function $f(x)$.

Now, when the transformation is defined we still have to define when the source and target images are registered. We can say that, the images $S(\overrightarrow{x})$ and $T(\overrightarrow{x})$ are perfectly registered if the function f satisfies the equation:

$$S(f(\overrightarrow{x})) \equiv T(\overrightarrow{x}) \tag{2}$$

To calculate whether the two images are equivalent, we have to define a similarity measure between the images $S(f(x), y)$ and $T(x, y)$, along with optimization algorithm that will maximize the similarity measure with respect to transformation function $f(x)$, i.e. find $f_{optimal}$. This can be written as:

$$f_{optimal} = max_f E(S(f(x), y), T(x, y)) \tag{3}$$

where E represents an image similarity measure and $f_{optimal}$ describes the optimal transformation function in the sense of the maximal similarity between $S(f(x), y)$ and $T(x, y)$, where only N degrees of freedom are allowed, since the transformation function is constructed out of the transformation vector.

Figure 1. Ten scaled segments of an image (left) and the same ten segments scaled with transformation function (right). See text for details.

Woods et al.[5] first presented mutual information as promising for intermodality registration, mainly because different medical imaging modalities usually have different medical intensities, characteristics and different resolutions. Mutual information is also described as a similarity measure that does not make any assumptions regarding the nature of the relation between the image intensities in the registered images.[6,7] Given that, when registering Doppler ultrasound images, we are interested in global correspondence and that these images are inherently containing a lot of (speckle) noise, we used mutual information in its normalized form:[6,8]

$$NMI(S,T) = \frac{H(S) + H(T)}{H(S,T)}, \tag{4}$$

where $H(S)$ and $H(T)$ stands for entropy of images S and T, and $H(S,T)$ for joint entropy.

For image registration, usually, the energy function consists of two parts. The first part measures the similarity of the images and the second part penalizes the warp. As the similarity measure the Normalized mutual information was selected which gave the form of the equation:

$$E(S(x),T(x)) = NMI(S(f(x),y),T(x,y)) - \alpha \cdot C(t) \tag{5}$$

The parameter α weights the second part and determines the trade-off between the similarity measure and the regularization. The selected value was 0.01 and the function $C(t)$ is defined as:

$$C(t) = \sum_{i=1}^{N-1} |t(i+1) - t(i)| \tag{6}$$

where N stands for the vector length (and corresponds to the number of vertical segments, as defined earlier), and $t(i)$ for the i-th element of the vector t.

Although transitivity and inverse consistency do not guarantee the accuracy of the registration they are often preferable or even used as measure of quality of the registration.[9,10] Since this is the unidirectional registration, the inverse consistency is not guaranteed. Therefore a modification of the first part of the Equation 5 is used instead.[9,11] If the images are already scaled to the same resolution, we can write this first part in the form:[12]

$$E_1(S,T,f) = NMI(S(x,f(x)\cdot y),T(x,y)) + NMI(S(x,y),T(x,f^{-1}(x)\cdot y)) \tag{7}$$

The energy function used as a similarity measure can therefore be written as:

$$E(S(x),T(x)) = E_1(S,T,f) - \alpha \cdot C(t) \tag{8}$$

In this study 59 images form 30 healthy volunteers were used. The number of segments selected for this study was 10 ($N = 10$). To maximize the function from the Equation 8, a genetic algorithm was used for the optimization. A 50 generations of 50 units with 40% probability of the crossover and mutation, were calculated on a cluster of PCs using Matlab and the Distributed Computing Toolbox. The final result was selected as the best one from the generations.

2.2 Model-based Segmentation

The idea of model-based segmentation is based on the use of a representative reference (or model) image, where the desired structure is manually segmented by an expert cardiologist. The desired structure is the aortic outflow velocity profile. This expert segmentation is done only once on the reference image, and is later used for automated segmentation. When a new patient image is acquired, the segmentation is conducted in two steps:

1. The reference image is registered to the new (target) image which must be segmented, resulting in a set of parameters describing the geometric transformation that is mapping the reference to the target image.
2. The aortic outflow profile from the reference image (the model) is geometrically transformed using the parameters obtained in the previous step. Since the reference image is already segmented, the obtained outflow profile after registration to a target image is the required segmentation.

In this paper, we used a representative image of a normal healthy volunteer as the reference image. As an representative the least different image (with respect to the transformation function) compared to all other images is selected. Rohfling et al.[13,14] in theirs works have used similar approach where just one individual was selected as a model image, where the criteria for selection of this image was different.

To find the image that is the least different form the rest of the images in the set it was necessary to calculate the mutual mappings of all the images. After this mapping all the transformation vectors from one image to any other image of the set is known. The distance function is now defined:

$$D(k) = \sum_{i=1}^{M} |I - t_{k \to i}|, \tag{9}$$

where M stands for number of the outflow profiles (i.e. $M = 59$), and $t_{k \to i}$ for the transformation vector of the k-th outflow profile onto the i-th. I denotes the identity transformation vector, i.e. the vector with all "ones", and represents no distortion of the image. Now we could easily extract k-th image that has smallest distance from the rest of the set.

3. EXPERIMENTS

3.1 Evaluation of Registration Method Using a Phantom

To estimate the registration accuracy, a phantom image was constructed. The outflow profile in it's first approximation can be seen as parabola in x-axis direction that declines with change of y. This was simulated using the following expression:

$$\begin{gathered} P : \mathbb{R}^2 \to \mathbb{R} \\ P(x,y) = \frac{1}{1+(x-c_1)^2} \cdot (c_2 - c_3 \cdot arctg(y - c_4)) \end{gathered} \tag{10}$$

The resulting image is shown in Figure 2 (left). Additionally, we defined a transformation vector t, which was used to construct the transformation function to deform the phantom. The deformed phantom constructed using the same deformation function which was implemented in the optimization algorithm and t defined as in Equation 11 is shown in Figure 2 (middle).

$$t = [1.3, 1.3, 1.2, 1.2, 1.1, 1, 1, 1, 0.9, 0.7] \tag{11}$$

After deformation the phantom was labeled as the target, and the deformed phantom as the source image. These two images were used as input parameters for our optimization algorithm. The registration method resulted in the transformation vector as shown in Table 1 (first row). In the second row, the Hadamard product of the vectors t and t_{op} is calculated, to check the inverse compatibility of these two vectors. The most right image in Figure 2 shows the deformed phantom image after it is re-transformed with the function constructed from t_{op}.

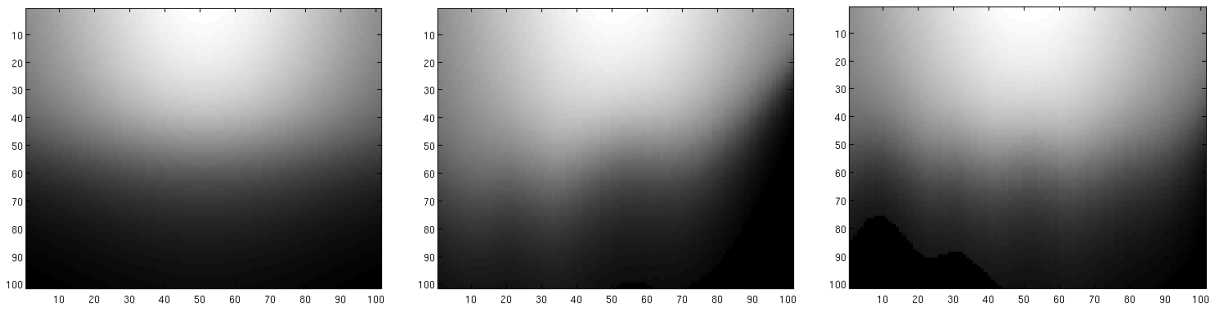

Figure 2. Phantom image, deformed phantom and inverse deformed phantom. All axis are in pixels.

t_{op}	0.8304,0.7657,0.8941,0.8825,0.9818,1.0414,1.0892,1.0672,1.1486,1.4080
$t_{op}. * t$	1.0795,0.9954,1.0729,1.0590,1.0799,1.0414,1.0892,1.0672,1.0337,0.9856

Table 1. Transformation vector and Hadamard product

If we denote as f_{op} the transformation function corresponding to t_{op}, than the re- transformed image can be described as $f_{op}(f(P))$. To see how each of these transformations affect the normalized mutual information, it was calculated for the three cases (shown in Table 2). It is interesting to note that the ideal inverse transformation function $f^{-1}(f(P))$, with a known transformation vector), does not reach the maximum possible value for the normalized mutual information. Nevertheless, from the Table 2 we can conclude that we may be satisfied with the transformation function as found by our optimization algorithm (f_{op}), since it produces the results close to the ideal inverse function (f^{-1}).

$NMI(P, f_{op}(f(P)))$	1.42
$NMI(P, f^{-1}(f(P)))$	1.68
$NMI(P, P)$	2.00

Table 2. Normalized mutual information

3.2 Clinical Evaluation of the Model-based Segmentation

For the purpose of this study the Continuous Wave Doppler traces of the aortic outflow, from 30 normal volunteers, were acquired with a clinical echocardiographic scanner (Vivid 7, GE Healthcare) using an apical 5-chamber view. Images were digitally stored in 'raw' Dicom format, containing the spectral Doppler information in proprietary tags. These 'raw' Dicom images were converted into Hierarchical Data Format (HDF) using an Echopac workstation (GE Healthcare). From the HDF file, the image containing the aortic velocities was extracted. To time the cardiac cycle, a single ejection period (from opening until closure of the valve) was manually indicated by an expert cardiologist. To ease this work, a software application was implemented with a graphical user interface as illustrated in Figure 3. From the 30 individuals included in the study, from all but one, two heart beats were acquired, resulting in a total of 59 outflow profiles used for processing.

The validation of the proposed model-based segmentation method was performed by comparing the automatic segmentation with a manual delineation performed by an expert cardiologist, who also manually segmented the reference (model) image. The manual segmentation was done using gimp,[15] and from this image, the border between regions are extracted as a function: $B : \mathbb{R} \rightarrow \mathbb{R}$. The reference image was subsequently registered to all the other images and the transformation functions were calculated and used to transform the border of the segmented model image onto the non-segmented image. In discrete form, this can be written as Hadamard product:

$$B_a[x] = f^{-1}[x]. * B_r[x] \tag{12}$$

where B_a represents the border of the outflow profiles of the normal volunteers obtained from the automatic segmentation, and B_r the boundary of the reference image. In order to evaluate the performance of this segmentation approach, the results (B_a) were compared to the best segmentation that could be provided in these

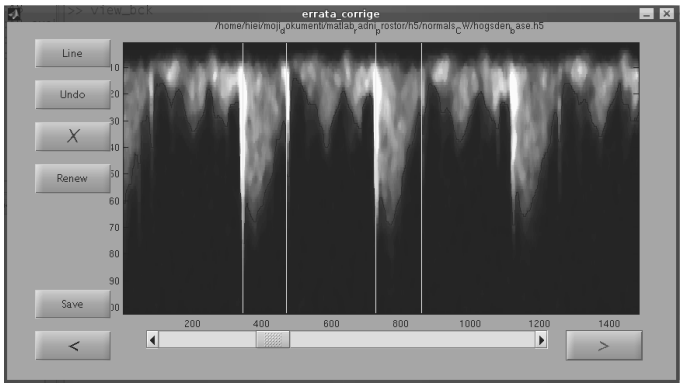

Figure 3. Illustration of graphical user interface used for indicating opening an closuring of the valve.

clinical images: the manual segmentation by the expert (denoted by B_m). For the brevity of presentation, only two of the images from the set of 59 images were selected as representative and shown in in Figure 4, where solid line represents manual and the dotted automatic segmentation.

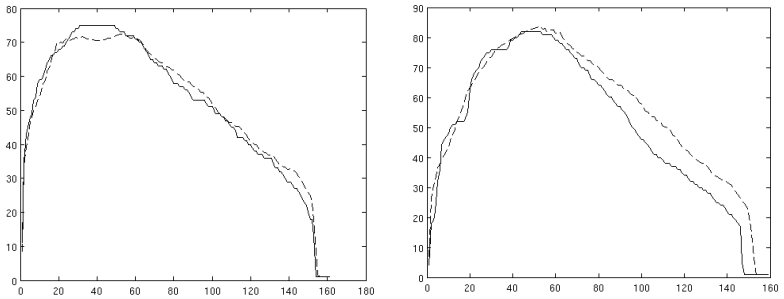

Figure 4. Transformation from the reference image to the manually segmented image. All axis are in pixels.

The average error (calculated as the sum of the absolute difference between the transformed reference border and the manually delineated border, divided by the resolution of the image, was 6.62%. To get an idea on the reproducibility of the manual segmentation, for a few cases, the error between two manually delineations by the same cardiologist (performed with some time gap in between) was calculated. This error was in some cases above 12%.

Additionally, to assess the quality of the segmentation, the homogeneity of the image intensities around the obtained delineation (the mean values with standard deviation) were calculated for both the manual and the automatic segmentation. Table 3 compares the mean intensities for the manually and automatically segmented border, with the mean intensities of the whole target image in the first column, and their standard deviation in the second. The notation $B_m\{i\}$ and $B_a\{i\}$ was used to denote the pixel set on which the manually and automatically segmented border lies on, while the notation $T(\overrightarrow{x})$ was used for the pixel set of the target image.

	$\bar{z}$	σ^2		$\bar{z}$	σ^2
$B_m\{i\}$	69.6667	27.1468	$B_m\{i\}$	60.1088	25.3334
$B_a\{i\}$	54.7093	15.3528	$B_a\{i\}$	59.2395	18.1734
$T(\overrightarrow{x})$	95.2149	84.0662	$T(\overrightarrow{x})$	79.1770	76.2523

Table 3. Mean pixel intensities ($\bar{z}$) and their standard deviation (σ^2) for the borders from Fig. 4 and the whole images. See text for details.

Table 4 shows the mean intensities for the manually and automatically segmented border of all images

alongside with their standard deviation and equivalent values for target image.

	$\bar{z}$	σ^2
$B_m\{i\}$	60.0012	35.1627
$B_a\{i\}$	50.5117	19.3723
$T(\overrightarrow{x})$	77.2987	70.2982

Table 4. Mean pixel intensities and their standard deviation for the manual and automatic segmentation on all images.

4. DISCUSSION AND CONCLUSION

In this paper, we introduced (i) a new method for the registration of Doppler ultrasound velocity images, and, using this registration approach, (ii) a new model-based segmentation of aortic outflow velocity profiles.

The phantom validation demonstrated that the registration is quite accurate, with an error of the transformation function, on average, around 5.4% (see Table 1). From the Table 2 we can conclude that the achieved maximum is close to optimal, since even the ideal inverse transformation does not reach absolute maximum of the normalized mutual information, which was used as similarity measure.

When the results of registration and automatic segmentation are compared to a manual segmentation by an expert cardiologist, the difference, as a measure of the error of the automated segmentation, is 6.62%, on average. Since the error, in most cases, is actually between 2 and 6 pixels (depending on the resolution of the image), this can partially be explained as a human error in the manual segmentation. Compared to the inter-observer error this error is within the tolerance values.

When the results of manual and automatic segmentation are compared, with respect to the variability of the intensity values (see Tables 3 and 4), it is easy to conclude that automatic segmentation has less deviations around mean values, i.e. that the thresholding is more consistent than the manual one.

Thus, we can conclude that the proposed method for the image registration can be used for the automatic segmentation of Doppler ultrasound images and that its average error is not larger than the inter-observer human error. Also this method is more consistent, in the sense of the intensity values variability.

REFERENCES

[1] Bijnens, B. H., Cikes, M., Claus, P., and Sutherland, G. R., "Velocity and deformation imaging for the assessment of myocardial dysfunction," *Eur J Echocardiogr* , jen323 (2008).

[2] Hatle, L. and Angelsen, B., eds., [*Doppler ultrasound in cardiology - Physical principles and clinical applications*], Lea & Febiger, Philadelphia, second ed. (1982).

[3] Bijnens, B., Claus, P., Parsai, C., Cikes, M., Loncaric, S., Anderson, L., and Sutherland, G., "An integrated framework for the assessment of cardiac function - description and illustrated applications," in [*Proceedings of the Fifth Int'l Symposium on Image and Signal Processing and Analysis*], 332–337 (2007).

[4] Kalinić, H., Lončarić, S., Čikeš, M., Baltabaeva, A., Parsai, C., Šeparović, J., Čikeš, I., Sutherland, G. R., and Bijenens, B., "Analysis of doppler ultrasound outflow profiles for the detection of changes in cardiac function," in [*Proceedings of the Fifth Int'l Symposium on Image and Signal Processing and Analysis*], 326–331 (2007).

[5] R. P. Woods, S. R. C. and Mazziotta, J. C., "Rapid automated algorithm for aligning and reslicing pet images," *Journal of Computer Assisted Tomography* **16**(4), 620–633 (1992).

[6] Maes, F., Collignon, A., Vandermeulen, D., Marchal, G., and Suetens, P., "Multimodality image registration by maximization of mutual information.," *IEEE Transaction on Medical Imaging* **16**, 187–198 (April 1997).

[7] Mäkelä, T., Clarysse, P., Sipilä, O., Pauna, N., Pham, Q.-C., Katila, T., and Magnin, I. E., "A review of cardiac image registration methods.," *IEEE Trans. Med. Imaging* **21**(9), 1011–1021 (2002).

[8] Hajnal, J. V., Hill, L. G., and Hawkes, D. J., eds., [*Medical Image Registration*], CRC Press, Cambridge, first ed. (2001).

[9] Christensen, G. E., Johnson, H. J., and Vannier, M. W., "Synthesizing average 3d anatomical shapes.," *Neuroimage* , 146–158 (2006).

[10] Lorenzen, P., Prastawa, M., Davis, B., Gerig, G., Bullitt, E., and Joshi, S., "Multi-modal image set registration and atlas formation," *Medical Image Analisys* **10**, 440–451 (June 2006).

[11] Christensen, G. and Johnson, H., "Consistent image registration," *IEEE Transactions on Medical Imaging* , 568–582 (2001).

[12] Skrinjar, O. M. and Tagare, H., "Symmetric, transitive, geometric deformation and intensity variation invariant nonrigid image registration," in [*ISBI*], 920–923 (2004).

[13] Rohlfing, T., Brandt, R., Menzel, R., and Maurer, C. R., "Evaluation of atlas selection strategies for atlas-based image segmentation with application to confocal microscopy images of bee brains.," *Neuroimage* **21**, 1428–1442 (April 2004).

[14] Rohlfing, T., Brandt, R., Menzel, R., Russakoff, D. B., and Maurer, Jr., . C. R., [*The Handbook of Medical Image Analysis – Volume III: Registration Models*], ch. Quo Vadis, Atlas-Based Segmentation?, 435–486, Kluwer Academic / Plenum Publishers (2005).

[15] "http://www.gimp.org/."